ORCA – Online Research @ Cardiff

Extremely low excess noise and high sensitivity AlAs$_{0.56}$Sb$_{0.44}$ avalanche photodiodes

Xin Yi[1,4], Shiyu Xie[2,4*], Baolai Liang[3*], Leh W. Lim[1], Jeng S. Cheong[1], Mukul C. Debnath[3], Diana L. Huffaker[2], Chee H. Tan[1], and John P. R. David[1*]

[1]Department of Electronic and Electrical Engineering, University of Sheffield, Sheffield, S1 3JD, UK.
[2]School of Physics and Astronomy, Cardiff University, Cardiff, CF24 3AA.
[3]California NanoSystems Institute, University of California-Los Angeles, Los Angeles, CA 90095, USA.
[4]These authors contributed equally: Xin Yi, Shiyu Xie.
*email: XieS1@cardiff.ac.uk; bliang@cnsi.ucla.edu; j.p.david@sheffield.ac.uk

Fast, sensitive avalanche photodiodes (APDs) are required for applications such as high-speed data communications and light detection and ranging (LIDAR) systems. Unfortunately the InP and InAlAs used at the gain material in these APDs have similar electron and hole impact ionisation coefficients (α and β respectively) at high electric fields, giving rise to relatively high excess noise, limiting their sensitivity and gain bandwidth product (GBP)[1]. Here, we report on extremely low excess noise in AlAs$_{0.56}$Sb$_{0.44}$ lattice matched to InP. The deduced β/α ratio as low as 0.005 in the avalanche region of 1550 nm is close the theoretical minimum and is significantly smaller than Silicon, with modelling suggesting that vertically illuminated APDs with a sensitivity of -25.7 dBm at a bit-error rate (BER) of 1×10^{-12} at 25 Gb/s at 1550 nm can be realised. The findings could yield a new breed of high performance receivers for applications in networking and sensing.

The advantages of using InP based APDs at traditional telecommunication wavelengths of 1310 nm and 1550 nm as a way of increasing sensitivity and speed of communication networks is well documented[2,3,4]. Such APDs utilise InGaAs lattice matched to InP substrates as the absorber and an InP or InAlAs gain (or multiplication) region in the Separate Absorption and Multiplication (SAM)-APD configuration. However due to the broadly similar β/α ratio in these materials, particularly at high fields, their sensitivity and GBP are limited, hampering their use as the bit rate increases beyond 10 Gb/s. The best results at 25 Gb/s to 50 Gb/s currently utilise $\leq$ 100 nm thick InAlAs multiplication regions and these provide a sensitivity of between -22.6 dBm to -10 dBm respectively at a BER of 1×10^{-12}[5-7]. There have been many attempts at improving the performance of APDs for telecommunications, for example utilising Ge/Si[8-10], nanopillars[11], AlInAsSb[12-14] or InAs[15], however these face problems such as limited wavelength operation, often requiring difficult growth procedures, complex fabrication technologies or the use of more expensive substrates. In this letter we demonstrate that the InP lattice matched alloy system AlAs$_{0.56}$Sb$_{0.44}$ with its very small β/α ratio[16] leads to extremely low excess noise at room temperature, even at high gains, exceeding the performance of all materials lattice matched to InP and even silicon. This extremely small β/α ratio changes the paradigm whereby high speed APDs always use very thin avalanching structures to one where both high speed and sensitivity can be achieved with thicker avalanching structures.

Three AlAs$_{0.56}$Sb$_{0.44}$ structures with avalanche region thicknesses of 1550 nm (P1), 660 nm (P2) and 1150 nm (P3) in a PIN configuration and two NIP structures with avalanche region thicknesses of 1550 nm (N1) and 660 nm (N2) were investigated. Fig. 1a shows a schematic diagram of P1 with

details of the other structures, the growth and fabrication techniques given in Method and Supplementary section 1. For comparison, two $AlAs_{0.56}Sb_{0.44}$ PIN structures with thin avalanche region thickness of 230 nm (P4) and 80 nm (P5) reported previously[17] were also measured. Figs. 1b and 1c show the multiplication (M) and the (M-1) data respectively obtained using different wavelength illumination on these avalanching structures as a function of reverse bias. By plotting (M - 1) on a log scale in Fig. 1b, we can see how the onset of the avalanche process changes with wavelength more clearly.

The excess noise (F) of the photocurrent when undergoing avalanche multiplication is shown in Fig. 2a-c. No excess noise data could be obtained on the two NIP structures with 420 nm illumination as there was very little pure hole initiated multiplication. The excess noise when electron initiate the multiplication is conventionally characterised by the k factor, defined by McIntyre[18] as the materials β/α ratio when $\alpha > \beta$ as $F_e = kM + (1 - k)[2 - 1/M]$. These are shown in Fig. 2a-c as dashed lines for different k values and to obtain low excess noise at high M, k has to be very low. When pure electrons initiate the avalanche process (Fig. 2a), the P1 and P3 show very low excess noise (F_e) corresponding to effective k values of 0.005 and 0.012, respectively. P2 demonstrates a larger effective k of 0.04 due to the higher electric field encountered and hence larger β/α, as shown by Yi et al.[16], a trend further exacerbated in P4 and P5 even with the advantage of dead space effects[19,20]. The F_e measured in 100 nm thick and 2500 nm thick InAlAs[21], currently the best lattice matched avalanche material for InP based telecommunication APDs, are shown in Fig. 2a. Commercially available silicon APDs have been reported with lower excess noise characteristics as shown in Fig. 2a but this requires very thick structures with high operating voltages[22]. Due to the large asymmetry in α and β, Fig. 2b and c show that the excess noise increases as the wavelength of illumination increases on the PIN structures with the opposite trend seen in the NIP structure as one might expect qualitatively. Results for P3 follow a similar trend as P1 and P2 (see Supplementary section 5). Under mixed carrier injection conditions, the F does not follow the theoretical McIntyre expression given earlier and there is currently no suitable model to predict this noise behaviour. Fig. 2d shows that the F_e results at M ~10 are in agreement with $AlAs_{0.56}Sb_{0.44}$ ionisation coefficients and McIntyre's model for P1-P3 structures suggesting the excess noise behaviour is dominated by β/α in $AlAs_{0.56}Sb_{0.44}$ avalanche regions > 660 nm but is reduced by dead-space effects for the two thinnest structures. Interestingly, bulk $In_{1-x}Al_xAs_{1-y}Sb_y$ on GaSb[12-14] also shows extremely low excess noise. The reduction in β there was attributed to high phonon scattering rates and the heavy effective hole mass associated with the large Sb component[13] and a similar mechanism may explain the results reported here on $AlAs_{0.56}Sb_{0.44}$.

Having demonstrated convincing experimental evidence of very small k values, we analyse the potential benefits of adopting $AlAs_{0.56}Sb_{0.44}$ in high speed APDs by undertaking a full bandwidth and sensitivity analysis on a number of design structures to estimate the theoretical performance of a typical SAM-APD. Such a model is sensitive to the exact parameters used so we have been relatively conservative in the assumptions of carrier velocity, dark current and the following trans-impedance amplifier (TIA) noise, the values of which are given in the Supplementary section 6. These structures have different thicknesses of $AlAs_{0.56}Sb_{0.44}$ multiplication regions, w_m, and the combined thicknesses of undoped InGaAs absorber, field control and grading layers, w_1. A Maximised-induced current (MIC)[7] absorber design (described in Methods) can provide for a responsivity of 0.92 A/W at 1550 nm and a responsivity of 0.69 A/W at 1310 nm while minimising the InGaAs absorber thickness. Carriers are created in the InGaAs layer according to the Beer-Lambert law after which they drift to the avalanche multiplication region. A Random Path Length (RPL) model[23] was used to simulate the

impact ionisation process within the multiplication region using ionisation path length probability distribution functions determined by experimental electron and hole ionisation coefficients[17]. With 50000 trails, we can obtain statistically accurate $M = <M_{trial}>$ and $F = <M_{trial}{}^2>/<M_{trial}>^2$ as a function of reverse bias. Assuming values of 1×10^5 m/s and 6.65×10^4 m/s for the electron and hole drift velocity respectively, and using Ramo's theorem[24] we can also obtain the mean current impulse response (see Fig. 3a). Fourier Transforming this mean current impulse response allows us to obtain the bandwidth (f_{3dB}) from the -3 dB point in the frequency response (see Fig. 3b). Fig. 3c shows the theoretically predicted GBP for AlAs$_{0.56}$Sb$_{0.44}$ APDs and measurement on an Al$_{0.85}$Ga$_{0.15}$As$_{0.56}$Sb$_{0.44}$ structure[24]. We undertook a similar GBP calculation for InAlAs APDs utilising the ionisation coefficients of InAlAs[21] and compared that to experimentally measured results[3,26-28] from the literature. The significantly larger GBP for AlAs$_{0.56}$Sb$_{0.44}$ APDs can be clearly seen and no significant improvement occurs for multiplication regions below 600 nm as the k value starts to increase. The sensitivity at a BER of 10^{-12} and an extinction ratio of 10 dB was calculated as described by Agrawal[29] and Ong et al.[30]. The receiver signal was determined by the average input optical power, P, and the diode responsivity, R. The total system noise was determined by the sum of noise power from the APD and the commercial available trans-impedance amplifier (TIA) noise as described in the Methods section. Fig. 3d shows the sensitivity achievable with different w_l at a wavelength of 1550 nm or 1310 nm and w_m of 1500 nm, 1000 nm and 600 nm for a BER of 1×10^{-12}. Fig. 3e shows the best sensitivity and speeds based on Si/Ge[8,10] and InGaAs/InAlAs[5-7,31] APDs that have been reported in the literature compared to the simulations in Fig. 3d. The modelled results in Fig. 3e suggest that even with 600 nm of w_m, we can operate the device at 1550 nm at 25 Gb/s with a sensitivity of -25.7 dBm as we can utilise a multiplication of ~9. By operating at 1310 nm with a thinner absorption layer, we can potentially operate in normal incidence with 600 nm of w_m at 40 Gb/s with a -20 dBm sensitivity and even at 50 Gb/s with a -15 dBm sensitivity. The predicted performance for the 2.5 and 10 Gb/s devices here are limited by the device surface dark currents and the TIA noise assumed, rather than factors such as the avalanche build-up time or the avalanche excess noise. In all cases, the significantly smaller k of AlAs$_{0.56}$Sb$_{0.44}$ compared to InAlAs enables a larger multiplication to be achieved before the speed is limited thereby improving the sensitivity.

In summary, the demonstration of low excess noise in AlAs$_{0.56}$Sb$_{0.44}$ enables a significant improvement in sensitivity in receivers operating at very high bit rates. For other applications like LIDAR, where speed is less of an issue, the much lower effective k values should enhance the signal to noise ratio of an AlAs$_{0.56}$Sb$_{0.44}$ based APD over existing material systems.

Methods

Epitaxial growth and device fabrication. The AlAs$_{0.56}$Sb$_{0.44}$ homojunction PIN/NIP structures are grown on epi-ready InP (001) substrates, via a digital alloy growth technique in a Veeco GEN930 MBE reactor, in which both As$_2$ and Sb$_2$ fluxes are controlled by using valved cracker cells. Standard metal ohmic contacts were deposited and optical lithography and wet chemical etching was used to fabricate mesa diodes. The exposed mesa sidewalls were passivated with SU-8. Further details of the growth and device fabrication can be found in Yi et al.[14] and in Supplementary section 1.

Absorption coefficient. The absorption coefficients were obtained by fitting to the external quantum efficiency based on current continuity equation (See Supplementary section 3).

Multiplication gain and excess noise. The multiplication and noise measurements were performed using 3 different wavelengths and a phase sensitive measurement technique as described by Li et al[19]. More details of the measurements undertaken and analysis is provided in Supplementary section 2.

Sensitivity analysis. The MIC absorber design[7] assumes a 500 nm undoped InGaAs providing a unity gain responsivity of 0.92 A/W at 1550 nm and a 100 nm undoped InGaAs providing a unity gain of 0.69 A/W at 1310 nm. Tan et al.[32] showed that it is possible to grade the heterojunction offsets and the electric-fields in an InGaAs-AlAs$_{0.56}$Sb$_{0.44}$ SAM-APD within 100 nm. The noise power from APDs, N_{APD}, is approximated by $N_{APD} = 2q \times (R \times P \times M + I_b \times M + I_s) \times M \times F \times f_{-3dB}$ where q is electric charge, I_b is the bulk leakage current and I_s is the surface leakage current, M is the avalanche multiplication, F is the excess noise factors, and f_{3dB} is the -3 dB bandwidth of the APD obtained by Fourier transforming the APD's impulse current response. The estimation of the APD's bulk and surface leakage current is based on the measured dark IV from different diameter devices as shown in Supplementary section 6. The carrier saturation drift velocity is similar to the values used to fit the gain-bandwidth product of a recently reported InGaAs-Al$_{0.85}$Ga$_{0.15}$AsSb SAM-APD[25]. Details of the TIA noise used are also given in the Supplementary Section 6. The BER was computed in the conventional manner[29,30] taking into account the mean and variance in the receivers output bit and setting the decision threshold at the middle.

Author contributions

S.Y.X., B.L.L. and J.P.R.D. designed the structures and B.L.L., M.C.D. and D.L.H. carried out layer growth. L.W.L. conducted the device fabrication. X.Y. undertook the experimental measurements. J.S.C. and X.Y. undertook the absorption modelling. S.Y.X performed the sensitivity simulations and SEM. X.Y., S.Y.X., C.H.T. and J.P.R.D. discussed and analysed the results, and wrote the manuscript. J.P.R.D., C.H.T. and D.L.H. supervised the project. All authors reviewed the manuscript and approved the paper.

Correspondence and request for materials should be addressed to J.P.R.D

Competing interests

The authors declare no competing interests.

Data availability

The data that support the plots within this paper and other findings of this study are available from the corresponding author upon reasonable request.

References

1. Emmons, R.B. Avalanche photodiodes frequency response. *J. Appl. Phys.* **38**, 3705 (1967).

2. Campbell, J.C. et al. Recent advances in avalanche photodiodes. *IEEE J. Sel. Top. Quantum Electron*. **10**, 777–787 (2004).

3. Nada M., Muramoto, Y., Yokoyama, H., Ishibashi, T. & Kodama, S. InAlAs APD with high multiplied responsivity-bandwidth product (MR-bandwidth product) of 168 A/W GHz for 25 Gbit/s high-speed operations. *Electron. Lett.* **48**, 397-399 (2012).

4. Nada, M., Yoshimatsu, T., Muramoto, Y., Yokoyama, H. & Matsuzaki, H. Design and performance of high-speed avalanche photodiodes for 100-Gb/s systems and beyond. *J. of Light. Technol.* **33**, 984-990 (2015).

5. Yoshimatsu, T. et al. Compact and high-sensitivity 100-Gb/s (4 x 25 Gb/s) APD-ROSA with a LAN-WDM PLC demultiplexer. *Opt. Express.* **20**, B393-398 (2012).

6. Shimizu, S., Shiba, K., Nakata, T., Kasahara, K. & Makita, K. 40 Gbit/s waveguide avalanche photodiode with p-type absorption layer and thin InAlAs multiplication layer. *Electron. Lett.* **43**, 476-477 (2007).

7. Nada, M. et al. 50-Gbit/s vertical illumination avalanche photodiode for 400-Gbit/s ethernet systems. *Opt. Express.* **22**, 14681-14687 (2014).

8. Kang, Y. et al. Monolithic germanium/silicon avalanche photodiodes with 340 GHz gain-bandwidth product. *Nat. Photonics.* **3**, 59-63 (2009).

9. Michel, J., Liu, J. & Kimerling, C. High-performance Ge-on-Si photometers. *Nat. Photonics.* **4**, 527-534 (2010).

10. Huang, Z. et al. 25 Gbps low-voltage waveguide Si-Ge avalanche photodiode. *Optica.* **8**, 793-798 (2016).

11. Farrell, A.C. et al. Plasmonic field confinement for separate absorption-multiplication in InGaAs nanopillar avalanche photodiodes. *Sci. Rep.* **5**, 17580 (2015).

12. Bank, S.R. et al. Avalanche photodiodes based on the AlInAsSb materials system. *IEEE J. Sel. Top. Quantum Electron.* **24**, 1-7 (2018).

13. Woodson, M.E. et al. Low noise AlInAsSb avalanche photodiode. *Appl. Phys. Lett.* **108**, 081102 (2016).

14. Rockwell, A. et al. $Al_{0.8}In_{0.2}As_{0.23}Sb_{0.77}$ Avalanche photodiodes. *IEEE Photonics Technol. Lett.* **30**, 1048-1051 (2018).

15. Marshall, A.R.J., Ker, P.J., Krysa, A., David, J.P.R. & Tan, C.H. High speed InAs electron avalanche photodiodes overcome the conventional gain-bandwidth product limit. *Opt. Express.* **23**, 23341-23349 (2011).

16. Yi, X. et al. Demonstration of large ionization coefficient ratio in $AlAs_{0.56}Sb_{0.44}$ lattice matched to InP. *Sci. Rep.* **8**, 9107 (2018).

17. Xie, J. et al. Excess Noise Characteristics of Thin AlAsSb APDs. *IEEE Trans. Electron Devices.* **59**, 1475-1479 (2012).

18. McIntyre, R.J. Multiplication noise in uniform avalanche diodes. *IEEE Trans. Electron Devices.* **ED-13**, 164–168 (1966).

19. Li, K.F. et al. Avalanche multiplication noise characteristics in thin GaAs p^+-i-n^+ diodes. *IEEE Trans. Electron Devices.* **45**, 2102-2107 (1998).

20. Hayat, M.M. et al. Effect of dead space on gain and noise of double-carrier-multiplication avalanche photodiodes. *IEEE Trans. Electron Devices.* **39**, 546-552 (1992).

21. Goh, Y.L. et al. Excess avalanche noise in $In_{0.52}Al_{0.48}As$. *IEEE J. Quantum Electron.* **43**, 503-507 (2007).

22. Hamamatsu. Produce datasheet: Si APD (S10341 series). Welwyn Garden City, U. K.

23. Ong, D.S.G. et al. A simple model to determine multiplication and noise in avalanche photodiodes. *J. Appl. Phys.* **83**, 3426 (1998).

24. Ramo, S. Currents induced by electron motion. *Proc. of IRE.* **27**, 584-585 (1939).

25. Xie, S. et al. InGaAs/AlGaAsSb avalanche photodiode with high gain-bandwidth product. *Opt. Express.* **24**, 24242-24247 (2016).

26. Rouvie. A. et al. High gain x bandwidth product over 140 GHz Planar junction AlInAs avalanche photodiodes. *IEEE Photon. Tech. Lett.* **20**, 455–457 (2008).

27. Li, N. et al. InGaAs /InAlAs avalanche photodiode with undepleted absorber. *Appl. Phys. Lett.* **82**, 2175–2177 (2003).

28. Hayashi, M. et al. Microlens-integrated large-area InAlGaAs–InAlAs superlattice APDs for eye-safety 1.5 mm wavelength optical measurement use. *IEEE Photon. Tech. Lett.* **10**, 576–578 (1998).

29. Agrwall, G.P. *Fber-optic Communication System Ch.4.* (John Wiley & Sons, Inc., USA, 1992)

30. Ong, D.S.G. et al. Optimisation of InP APDs for high-speed lightwave systems. *J. Light. Technol.* **27**, 3294-3302 (2009).

31. Ishimura, E. & Yagyu, E. High sensitivity 2.5/10 Gbps InAlAs avalanche photodiodes. *Mitsubishi Electr. Adv.* **127**, 17-29 (2009).

32. Tan, C.H., Xie, S. & Xie, J. Low noise avalanche photodiodes incorporating a 40 nm AlAsSb avalanche region. *IEEE J. of Quantum Electron.* **48**, 36-41 (2012).

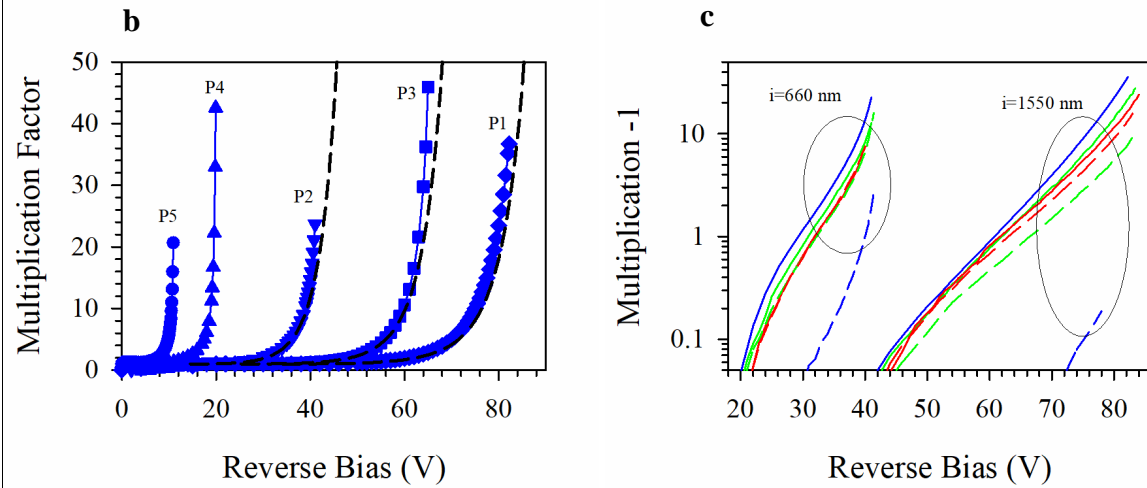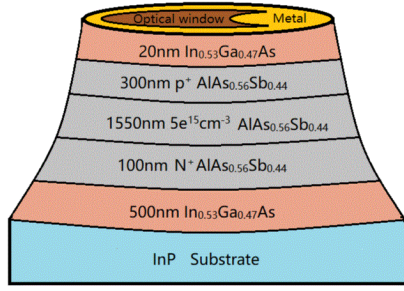## Acknowledgements

Section for figure captions

Fig. 1. Schematic diagram of P1 and measured multiplication results. a, Schematic diagram of the P1 mesa device with 220 μm diameter. b, Measured multiplication at 420 nm wavelength versus applied reverse bias for the PIN structures. The dashed lines are the theoretical values when $k = 0$. c, Measured multiplication at different wavelength (420 nm – blue, 543 nm – green and 633 nm – red) versus applied reverse bias for the 660 and 1550 nm PIN (solid lines) and NIP structures (dashed lines). The quantum efficiency of these samples as a function of wavelength is shown in Supplementary section 3.
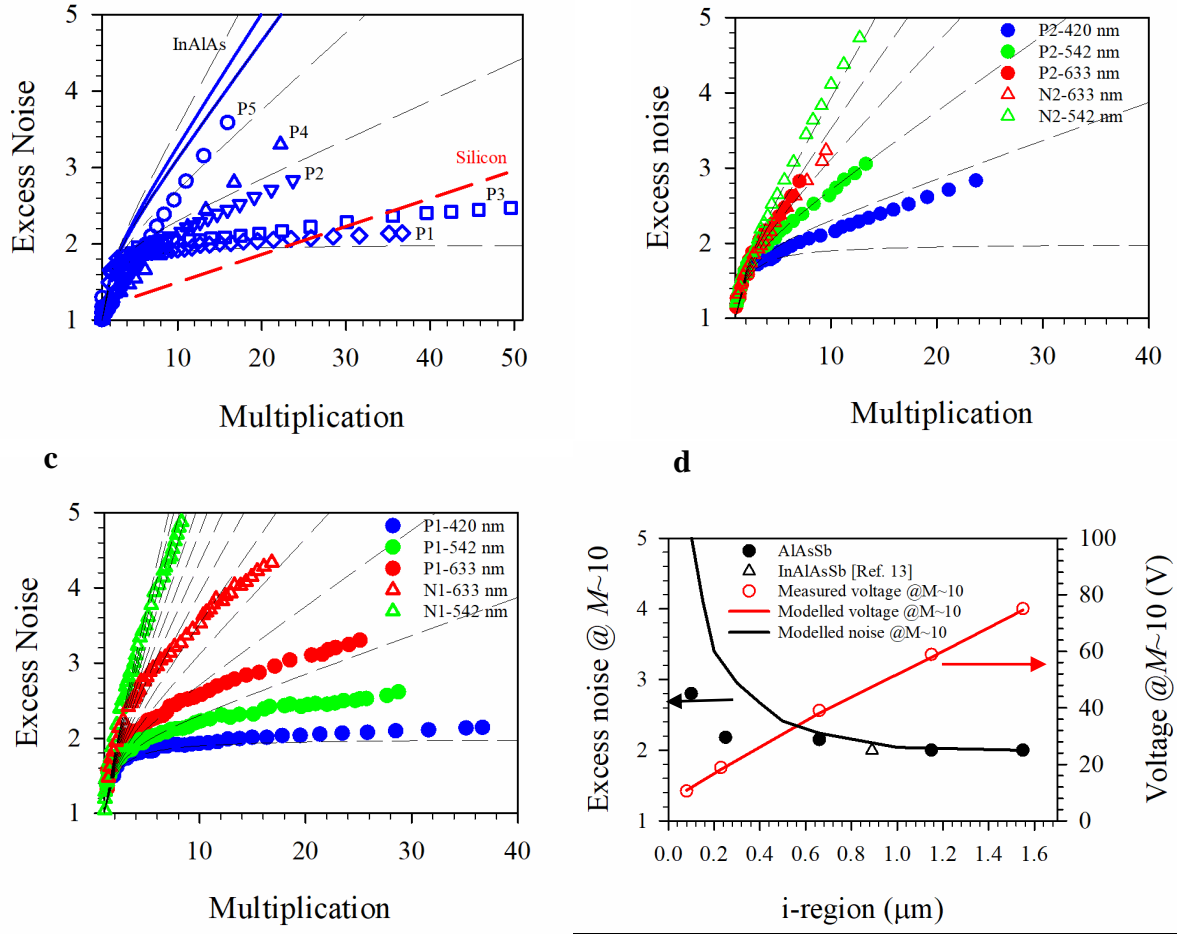
Fig. 2. Measured excess noise results. a, Measured excess noise versus multiplication with 420 nm illumination on all PIN structures compared with reported excess noise in InAlAs[21] and a commercial Si APD[22]. b, Measured excess noise versus multiplication at different wavelengths for the 660 nm PIN and NIP. c, Measured excess noise versus multiplication at different wavelengths for the 1550 nm PIN and NIP. d, The excess noise and applied voltage (at M ~10) versus avalanche width for AlAs$_{0.56}$Sb$_{0.44}$ PINs with 420 nm illumination and the InAlAsSb result from Woodson[13]. The black and red symbols are the measured excess noise and voltages for M ~10 while the lines are McIntyre's local model calculation for the excess noise (black) and the breakdown voltage (red). The grey dashed lines in (a)-(c) are calculated McIntyre's excess noise for different k increasing from 0 in steps of 0.05.
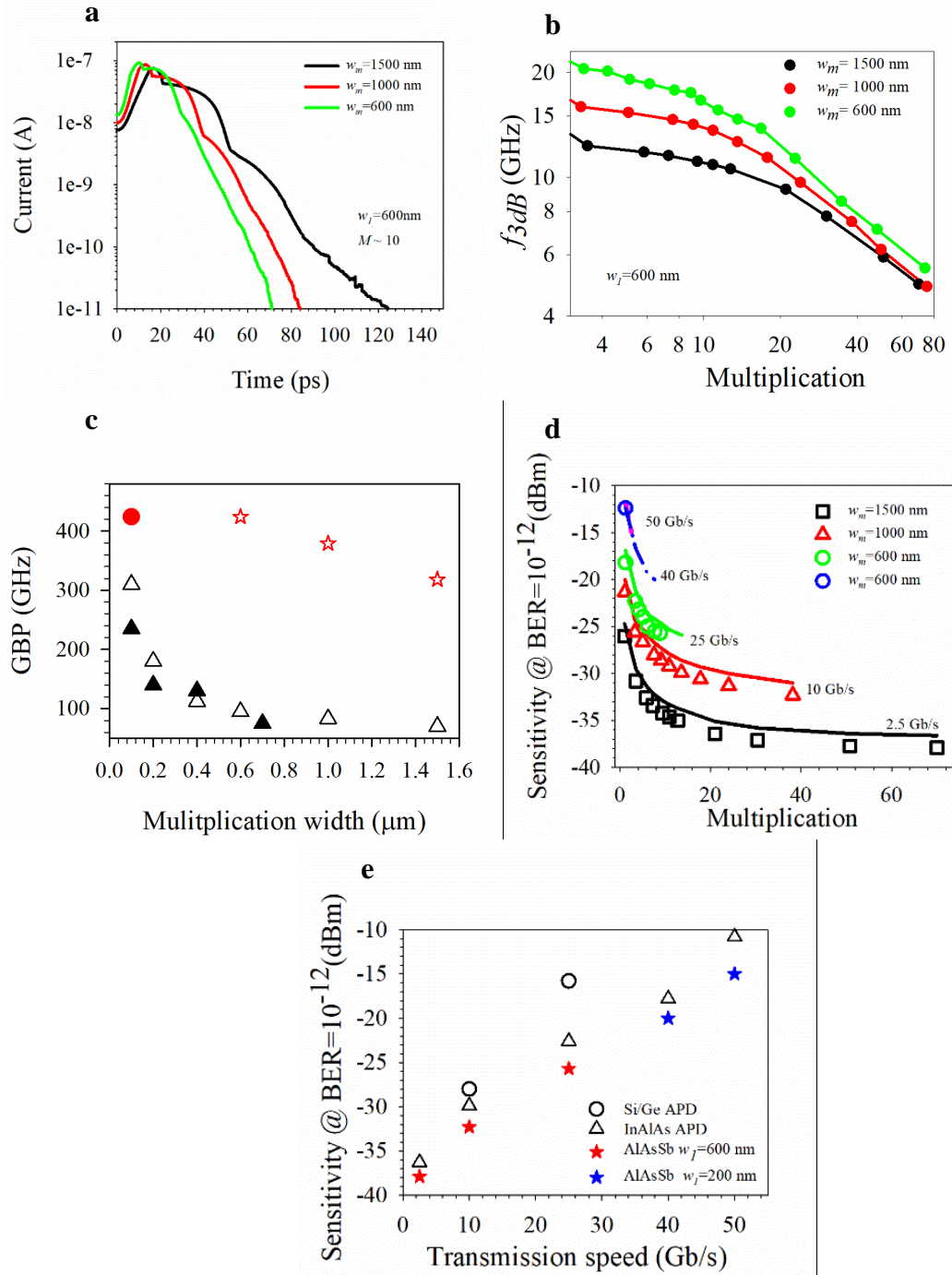
Fig. 3. Optical sensitivity modelling. a, The calculated mean current impulse response at $M \sim 10$. b, The predicted f_{3dB} versus M for AlAs$_{0.56}$Sb$_{0.44}$/InGaAs APD characteristics as a function of w_m. c, The predicted GBP for AlAs$_{0.56}$Sb$_{0.44}$ APD (red star), and InAlAs APD (open triangle). The measured GBPs for InAlAs APD[3,25-27] are also included for comparison (closed triangle) as is the measured GBP for Al$_{0.85}$Ga$_{0.15}$As$_{0.56}$Sb$_{0.44}$[25] (closed circle). d, InGaAs/AlAs$_{0.56}$Sb$_{0.44}$ APD sensitivity with $w_l = 200$ nm (lines) and 600 nm (symbols) for different w_m were simulated at 1550 nm (2.5, 10 and 25 Gb/s) and 1310 nm (40 and 50 Gb/s). e, The sensitivity potentially achievable in InGaAs/AlAs$_{0.56}$Sb$_{0.44}$ based APDs with $w_l = 200$ nm and 600 nm compared with Si/Ge[8,10] and InGaAs/InAlAs APDs[31]. The reported InGaAs/InAlAs APDs at 25[5] and 50 Gb/s[7] operated at 1310 nm. The 40 Gb/s[6] InGaAs/InAlAs APD result is for a waveguide structure while others are normal incidence structures.

9